Steel and Composite Structures, Vol. 5, No. 1 (2005) 49-70
DOI: http://dx.doi.org/10.12989/scs.2005.5.1.049

Finite element modeling of tubular truss bearings

B. Kozy† and C. J. Earls‡

Department of Civil & Environmental Engineering, University of Pittsburgh, Pittsburgh, Pennsylvania, 15222, U.S.A.

(Received November 2, 2004, Accepted January 10, 2005)

Abstract. This paper reports on finite element analysis techniques that may be applied to the study of circular hollow structural sections and related bearing connection geometries. Specifically, a connection detail involving curved steel saddle bearings and a Structural Tee (ST) connected directly to a large-diameter Hollow Structural Section (HSS) truss chord, near its open end, is considered. The modeling is carried out using experimentally verified techniques. It is determined that the primary mechanism of failure involves a flexural collapse of the HSS chord through plastification of the chord wall into a well-defined yield line mechanism; a limit state for which a shell-based finite element model is well-suited to capture. It is also found that classical metal plasticity material models may be somewhat limited in their applicability to steels in fabricated tubular members.

Key words: tubular truss; truss bearing; pipe bearing; pipe crushing; curved saddles; nonlinear finite element analysis.

1. Background

The focus of the research work reported on herein concerns bearing regions in long-span trusses composed of tubular members. Specifically, a connection detail involving curved steel saddle bearings and a Structural Tee (ST) connected directly to a large-diameter Hollow Structural Section (HSS) chord, near its open end, is considered (see Fig. 1). For simple-span HSS trusses, the primary load path for the reaction force developed at the support is from the bearing, through the chord, and directly into the first intermediate vertical member. Therefore, the overall connection capacity is influenced by all of these member proportions and their spacing with respect to one another. It is pointed out that in this research, the connection region is being investigated locally and without involving the global behavior of the entire truss (i.e., the more complicated member internal forces, resulting from effects of the structural system surrounding the connection detail, are not considered in this work). The assumption is that the effects of such additional internal forces are of small magnitude and hence will not significantly influence the local limit states under investigation. In considering this simplified loading condition, it is noted that while some research has been done on local concentrated loads applied to HSS walls through gusset plates (Kurobane 1976), very little work has been done on loads applied directly through the ends of an open rolled sections; no previous work has been found in the literature concerning the cases of saddle-type bearings located at chord ends or an ST bearing on a circular HSS chord.

†Adjunct Lecturer
‡Chairman and Associate Professor, Corresponding author, E-mail: earls@engr.pitt.edu

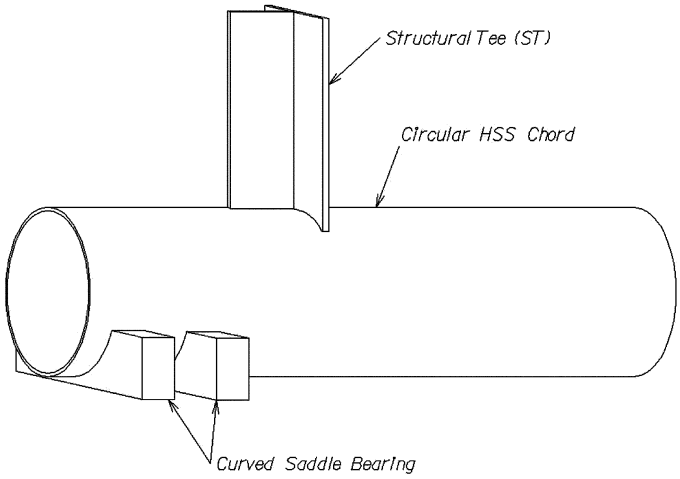

Fig. 1 Bearing connection detail under investigation

This current research is focused on the application of sophisticated nonlinear finite element modeling techniques, as well as full-scale experimental testing, for the quantification of truss end bearing connec-tion capacities. The nonlinear finite element modeling techniques employ experimentally verified strategies (previously verified against available relevant tests on tubular structures found in the literature as well as those tests carried out as part of the current research) and will form the cornerstone for future parametric studies carried out in support of the formulation of a design equation aimed at predicting bearing strength in circular HSS trusses. The full-scale tests carried out as part of the current research were executed using geometric configurations identified as either being most critical, or most germane, vis-à-vis initial parametric finite element analyses based on common U.S. design practice (PennDOT 2003a,b).

The purpose of the present paper is to discuss important modeling considerations and strategies required for the adequate treatment of the connection geometries that are at the heart of this finite element modeling effort.

2. Experimental testing

Full-scale portions of the bearing region of a particularly large tubular truss were instrumented and tested to failure in the Watkins-Hagaart Structural Engineering Laboratory at the University of Pittsburgh Main Campus in August 2003. Two (2) identical specimens were tested under identical loading conditions to ensure repeatability. These specimens were designed exactly to match a standard detail used in the case of a “tri-chord” sign structure spanning 60 m (197’) as specified in the *Standard Drawings for Bridge Construction [and Design]* (PennDOT 2003a,b). The specimens employ a combination of a 660 mm (26”) O.D. circular HSS chord member having a 12.7 mm (0.5”) wall thickness and a ST255x71.5 (ST10x48) vertical member oriented normally to the side wall of the HSS and bearing directly upon it. Also as specified in the *Standard Drawings for Bridge Construction* (PennDOT 2003b), the specimen was supported on two saddles that are proportioned and positioned within the load frame. Generally, the testing set-up is designed to closely represent the bearing geometry and loading configuration present in an actual field installation (see Fig. 2).

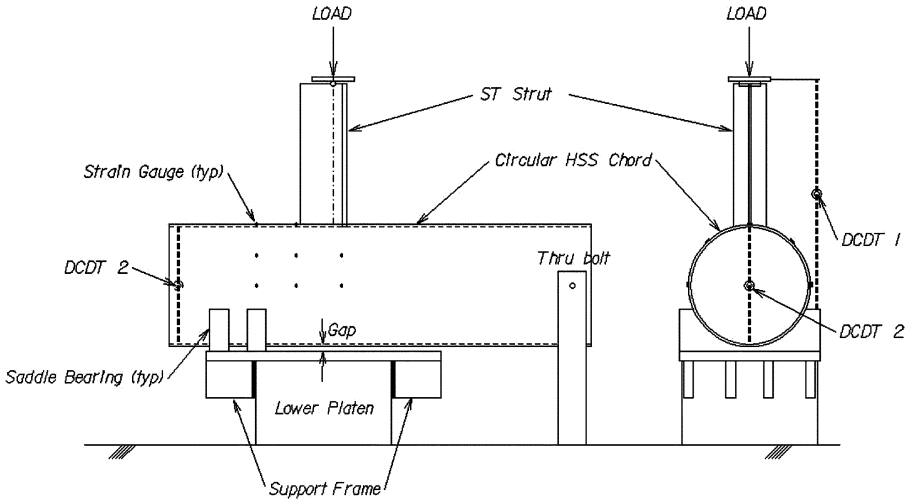

Fig. 2 Schematic of experimental test setup

The data set from the experimental testing is used for validation of nonlinear finite element modeling techniques to prove their viability for use in future studies. In particular, deflection and strain measurements made during the experimental testing are compared to those predicted by finite element analysis. For more detailed information on the experimental testing, see the report by Boyle and Earls (2004).

3. HSS material behavior

Since the experimental tests involve a concentrated load which essentially “crushes” the HSS chord, the overall response of the test specimens is very sensitive to the HSS material behavior. If the HSS material is not modeled correctly, then agreement between the experimental and finite element analysis results will be poor. Therefore, a number of issues relevant to HSS members, and their potential influence on the steel material behavior, are discussed below.

4. Standard mill practice

A common method for manufacturing circular steel HSS members and the method used for the test specimen chords is the “formed-from-round” process. This involves conversion of a flat steel plate into an HSS through a series of forming operations. As illustrated in Fig. 3, a flat strip of steel plate is bent continuously around its longitudinal axis to form an open-seam round by passing it through a progressive set of rolls. The resulting open-seam round is then closed with a continuous longitudinal weld. After welding, the section is cooled and then run through an additional set of sizing rolls to achieve the desired final shape (AISC 1997a). This is important to note since the cold working in these operations causes changes in stress-strain behavior from the basic steel material properties. A metal which has undergone a severe amount of deformation, as in rolling or drawing, will develop a

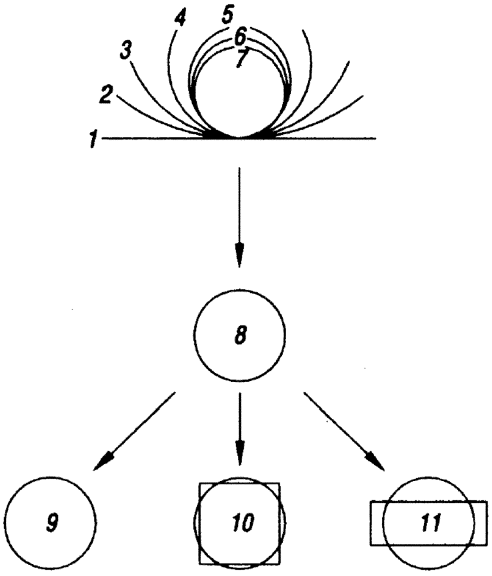

Fig. 3 Formed-from-round process (AISC 1997a)

preferred orientation, or "texture," in which certain crystallographic planes, or mechanical fibers, tend to orient themselves in a preferred manner with respect to the direction of maximum strain (Dieter 1986). Researchers have confirmed that this effect can be significant in tubular members by comparing the stress-strain behavior in steels from tubular columns with and without annealing (Popov *et al.* 1979).

5. Specifications

The HSS chords used in the test specimens were manufactured under ASTM A53: *Standard Specification for Pipe, Steel, Black and Hot-Dipped, Zinc-Coated, Welded and Seamless*. This specification is intended for mechanical and pressure applications and is also acceptable for ordinary uses in steam, water, gas, and air lines. It is suitable for welding, and suitable for forming operations involving coiling, bending, and flanging. However, ASTM A53 is not necessarily meant for structural applications in buildings and bridges as is the more common ASTM A500 *Standard Specification for Cold-Formed Welded and Seamless Carbon Steel Structural Tubing in Rounds and Shapes*. ASTM A53 Grade B was selected since this is the material specification used in Pennsylvania for fabrication of overhead sign trusses. The specification tensile requirements are as follows:

Min. Yield Strength = 241 MPa (35 ksi)
Min. Tensile Strength = 414 MPa (60 ksi)

6. Tolerances

Variations in geometric dimensions from the nominal values specified for the HSS members can have a significant affect on the behavior of the structure under investigation. The tolerances for fabrication of tubular members in general are not stringent as compared to similar open rolled structural shapes, and ASTM A53 is even more forgiving to manufacturers. The permissible variations as per ASTM A53 that should be noted are as follows:

HSS Outside Diameter: +/- 1%
HSS Wall Thickness: -12%
Straightness: No requirement
Mass (weight): +/- 10%

As a result of these generous tolerances, most HSS manufacturers tend to produce under-sized sections, but still within the specification limits (Packer 1997). Since connection capacity in tubular structures is typically a function of HSS wall thickness squared, the structural safety index can be very sensitive to this geometric property. As a result, the AISC HSS Specification (AISC 2000) states that a design wall thickness of 0.93 times the nominal thickness should be used for design calculations.

7. Residual stresses

Residual stresses in HSS members most commonly arise from the cooling effects after hot finishing, from the welding processes employed, or by the prevention of spring-back introduced during forming operations (Galambos 1998). Recalling the numerous forming and welding operations that a steel plate must be subjected to for creation of a tubular section by the formed-from-round method, it can be seen why significant residual stresses can develop. As a result of these operations, the exact shape of the stress-strain curve, the proportional limit, and the yield strength of tubular members can be somewhat unpredictable. Measurements on members fabricated for a column testing program (Chen and Ross 1977) gave the longitudinal and through-thickness circumferential residual stress patterns shown in Fig. 4. These patterns and general magnitudes have been confirmed by other researchers (Prion and Birkemoe 1988). The distributions show that significant residual stresses develop in tubular members; approaching 35% of the yield stress s_y in the circumferential direction and 100% of the yield stress in the longitudinal direction. It is noted that while the longitudinal residual stresses vary based on the distance from the seam weld, the circumferential residual stresses were found to be nearly the same in all locations around the perimeter (Toma and Chen 1979).

8. Coupon testing

Determining the mechanical properties of steel in HSS members can be problematic. Conventional coupon tests are possible for the longitudinal direction with some machining of the coupon, but not for the transverse direction due to the circular cross-section. To conduct a transverse tensile test (as per ASTM A370 *Standard Test Methods and Definitions for Mechanical Testing of Steel Products*), a ring must be cut from the specimen and then flattened. However, these test specimens require normalization due to this additional treatment.

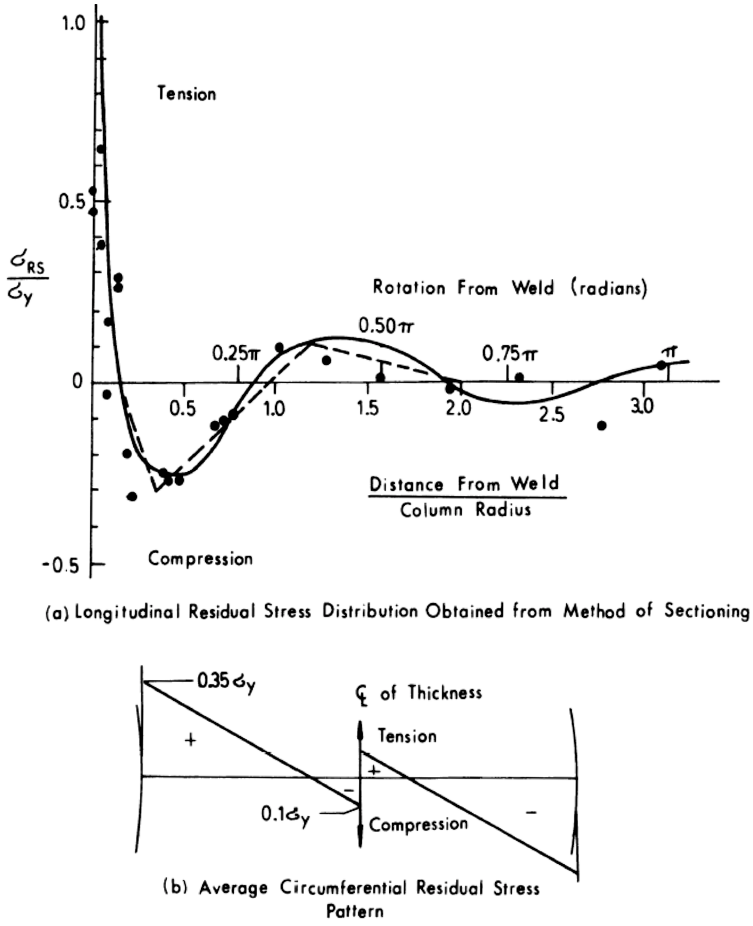

(a) Longitudinal Residual Stress Distribution Obtained from Method of Sectioning

(b) Average Circumferential Residual Stress Pattern

Fig. 4 Residual stresses in fabricated round tubular members (Toma and Chen 1979)

One of the unique features in the mechanical behavior of steels from tubular members is that the stress-strain response becomes nonlinear at low stresses and the yield point is typically not well defined as compared to conventional rolled steels. Toma and Chen attributed this to the residual stresses present in tubular members and developed the concept of the *Effective Young's Modulus* for describing the material response, for which a variable modulus is used to describe the slope of the complete stress-strain curve (Toma and Chen 1979). For this approach, the effective modulus is a function of the applied stress, the yield stress, and an *initial yield stress*, which results from the residual stresses present.

9. Finite element modeling techniques

The techniques employed for the finite element modeling are based on the techniques that were developed and validated by Li and Earls for earlier work on HSS connections (Li and Earls 2002). Consistent with this earlier work, the current research employs dense meshes of nonlinear shell finite

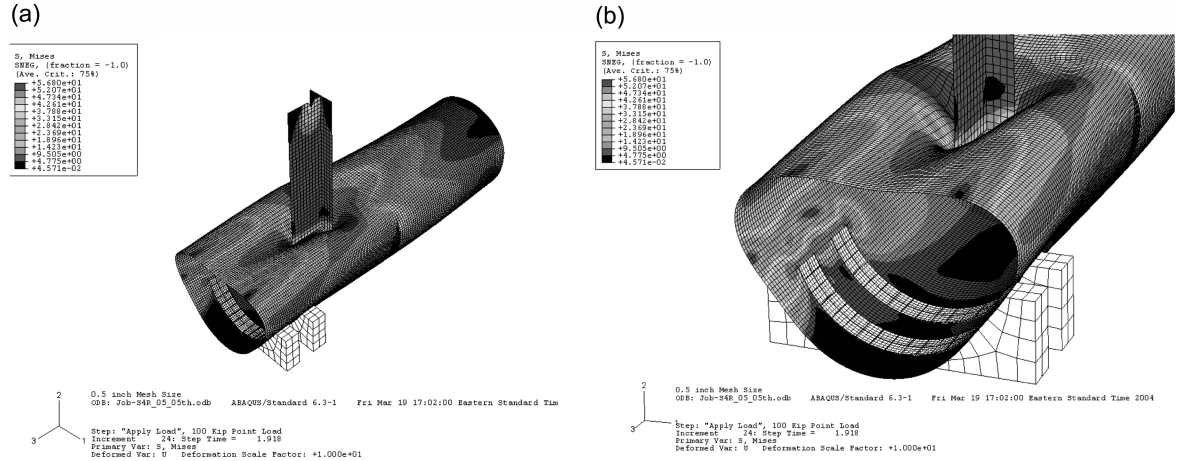

Fig. 5 Finite element model showing deformed shape and von Mises stress contours

elements positioned at the mid-surface of the constituent plate components for each of the structural members comprising the connection under investigation. The application of shell elements in this fashion permits the actual three-dimensional geometry of the structure to be replicated in a physically meaningful way.

Since the finite element models are to be used as the vehicle by which the response characteristics of multiple HSS truss connection geometries are to be quantified, it is important to ensure the robustness and viability of the modeling strategies adopted in the present work. As a means of validating these modeling techniques, they are first applied to the case of two full-scale experimental specimens tested as part of the current research effort. Favorable agreement between the modeling results of these specimens and the laboratory results are obtained. A detailed discussion of this comparison follows in a subsequent section of this paper.

Since the potential for steel yielding and localized buckling effects are present, the finite element modeling approach adopted considers both geometric and material non-linearities within the context of an incremental analysis. Thus, a Riks-based solution approach (ABAQUS 2003) is employed to capture both the intermediate loading steps leading up to the ultimate load as well as the response in the unstable (un-loading) region of the equilibrium path. The completed model of the experimental test in its deformed configuration at the ultimate load and with the von Mises stress contours displayed, in a magnified state, is shown in Fig. 5.

10. Boundary conditions and loading

For the boundary conditions and loading, there are a number of important features of the model that should be discussed. First, the interface between the saddles and the HSS is modeled as a fully pinned surface (i.e., every node at the interface between the HSS and the saddle is prevented from any translation). Thus, the HSS cannot separate from the saddle bearings or slide within the saddles. This is clearly an idealization of the true physical boundary condition, but was nonetheless found to be accurate (see discussion on Contact below) vis-à-vis the verification work carried out as part of the

current research. At the opposite (right) end of the structure, one node on each side of the HSS chord surface at mid-height is pinned to simulate a thru-bolt support condition used in the experimental testing. Finally, the unconnected end of the ST member, at the point of load application, is prevented from any lateral translation; consistent with the physical boundary condition in the test specimens. In addition, loading is imposed on the model through the application of a concentrated force at the centroid of the ST cross-section.

11. Element type

Since this structure consists of relatively thin components (some with curvature) subjected to primarily flexural and membrane stresses, the shell element is deemed to be the most appropriate finite element for use in the modeling. In general, the failure mechanism involved in this type of connection is seen to involve a plastic collapse of the HSS chord wall as a result of the formation of a system of well-defined yield lines. While it is that the structural element formulation employed in shell element formulations is well suited to capturing this type of behavior, it should be noted that the regions of the HSS chord in the vicinity of the ST are also observed to be subjected to large local transverse shear stresses as the applied load is transferred from the ST to the chord; a condition where even the most robust shell formulation may experience difficulties.

In choosing the specific shell element to be used in the modeling, several different types from the ABAQUS library are considered initially: S4, S4R, S8R, and STRI3. All of these shell elements utilize 6 degrees of freedom (DOF) at each node (3 translational and 3 rotational), but each is somewhat different in terms of its *formulation, integration*, and/or *interpolation*.

The shell *formulation* refers to the mathematical theory used to define the element's behavior. Shell problems generally fall into one of two categories: thin shell problems and thick shell problems. For a detailed discussion on different shell formulations, as well as proper integration order for the integration of their stiffness matrices, the reader is referred to the book by Bathe (1996). What follows now is a superficial discussion meant only as a summary of relevant concepts used in the present work. Thick shell problems assume that the effects of transverse shear deformation are important to the solution. Thin shell problems, on the other hand, assume that transverse shear deformation is small enough to be neglected. Thin shell elements provide solutions to shell problems that are adequately described by classical (Kirchhoff) plate theory, thick shell elements yield solutions for structures that are best modeled by shear flexible (Mindlin) plate theory. The STRI3 shell in ABAQUS is a thin shell element, the S8R is a thick shell, and the S4 and S4R are general-purpose shell elements. In ABAQUS so-called "general purpose" shell elements are considered valid for use in both thick and thin shell problems.

It should be noted that in the S4 and S4R shells, changes in the cross-section thickness, as a function of membrane strains and material definition are considered. This capability can be important in nonlinear analyses where large strains accompany large rotations. The shell kinematics for these two elements is based on an assumed-strain formulation that provides accurate solutions to many loading conditions, including in-plane bending behavior (ABAQUS 2003).

The shell *integration* refers to the number of discrete points within each element that are utilized to calculate the internal strain energy in the deformed configuration. Shell elements can be either fully integrated (e.g., S4, STRI3) or use reduced integration (e.g., S4R, S8R). For full integration, the standard Gauss quadrature is employed which results in four (4) integration points for a quadrilateral and three

Table 1 Summary of shell elements considered

ABAQUS Name	#Nodes/El	Formulation	Integration	Interpolation
S4	4	Gen. Purpose	Full	Linear
S4R	4	Gen. Purpose	Reduced	Linear
S8R	8	Thick	Reduced	Quadratic
STRI3	3	Thin	Full	Linear

(3) integration points for a triangular element. For reduced integration, only a single integration point is used for each of these elements. Reduced integration elements are attractive because they reduce computational expense while providing a means for mitigating shear locking effects which become pronounced when shear deformable shell formulations are used in situations where the through-thickness dimension is small. However, reduced integration elements often exhibit another numerical problem called hourglassing, in which the element can deform in certain ways with the internal strain energy remaining zero. Thus, fully integrated elements are recommended for conditions where greater solution accuracy is desired, or for problems where in-plane bending is expected (ABAQUS 2003). In all cases, five (5) Simpson integration points through the element thickness are utilized for tracking through-thickness plastification of the shell element cross-section.

The shell *interpolation* refers to the displacement functions that are assumed in the element formulation for describing the deformed shape between the element nodes. In the context of our present discussion, the interpolation order is either linear or quadratic. Quadratic elements are more accurate on a per element basis; however their use comes at an increased computational expense since additional nodes are required to adequately describe their shape.

A summary of the different shell elements considered and their respective features is shown in Table 1.

As part of the current research effort, an evaluation of element performance within the context of the current problem is undertaken. To complete this evaluative effort, analyses of the subject problem are conducted utilizing each of the four (4) elements identified in Table 1 and the model response characteristics are compared in the context of global load-deflection response as measured by DCDT 1 (see Fig. 6). For each of the finite element analyses, the geometry, boundary conditions, loading, and material model are identical. However, the finite element meshes vary slightly as a result of differences in elemental node layout. This is important to note since the solution is dependent upon the mesh density (# elements / unit area) as discussed below. To properly assess the relative performance of the four (4) shell elements, the mesh density is doubled for the STRI3 model and halved for the S8R model (as compared with the 4 node quadrilateral shell mesh). This results in the same number of nodes and DOFs for all four models.

In general, it can be seen that the load-displacement response is very similar for all the element types. As expected theoretically, all models predict the same result in the elastic range. It is not until well into the plastic range where some subtle differences arise. It is observed that the general-purpose shell elements (S4, S4R) show a slightly higher peak load than the two special purpose elements (S8R, STRI3) by approximately 2%. This is likely due to the consideration of finite membrane strains (greater than 1%) in the S4 and S4R formulations. During the analyses, strains of greater than 1% are observable in regions of the mesh where yield lines formed. In addition, since the HSS chord is subjected to compressive hoop stress as the load travels from the ST to the saddles, the shell thickness will increase by the Poisson effect as inelastic deformation occurs. This increase in thickness will have a strengthening effect on the yield line failure mechanism since the flexural strength (plastic moment

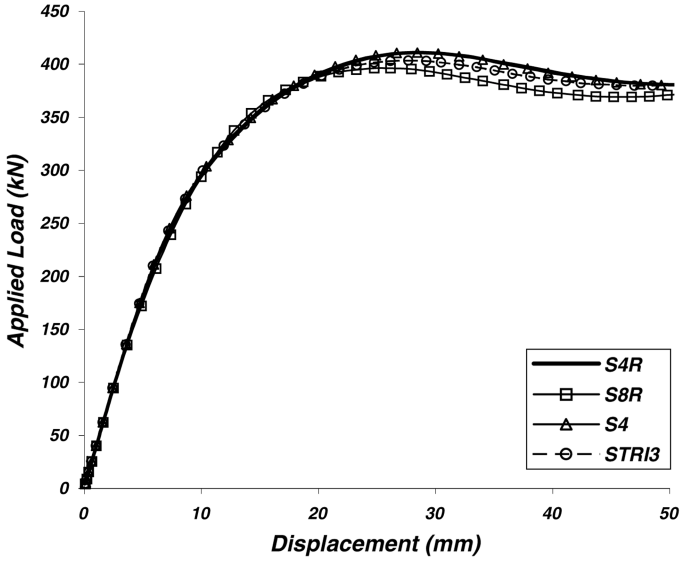

Fig. 6 Effect of element formulation on predicted response at applied load (DCDT 1)

capacity) is a function of the wall thickness. This strengthening effect was confirmed by performing a subsequent analysis with $\nu = 0$, for which the capacity was reduced to nearly the same value as given by the STRI3.

The second observation to make is that the S4 and S4R models predict nearly the same response throughout. This indicates that the reduced integration does not have a significant impact on the solution, which is good news since the run time is less for the S4R model.

The last observation is that the two special purpose elements (S8R, STRI3) predict similar responses even though the S8R is based on a thick shell formulation and the STRI3 is based on a thin shell formulation. This indicates that the problem is truly a thin shell problem, since reduced integrated thick shell elements like the S8R can have limited success solving a thin shell problem. The converse is not typically true for elements formulated for thin shell applications.

Based on this investigation, the S4R nonlinear, finite strain, general-purpose quadrilateral shell element from the ABAQUS element library is selected. A single integration point is used in this particular element, so computational expense is relatively low. Also, since consideration of finite membrane strains may be important to the behavior the structure under investigation, the S4R is the preferred choice. Furthermore, the authors have found the S4R element to produce reliable results for modeling of similar steel plate-type structures (Li and Earls 2002) (Thomas and Earls 2003) (Greco and Earls 2003).

12. Contact

Frequently, stresses developing at contacting interfaces between structural components in a system may prove to dominate an analysis. Such intense stress states may admit the possibility for interfacial slip, separation, and/or sliding as a result of stress concentrations, load redistribution, or other local mechanism. Therefore, there may be a danger that using a simplified modeling approach in the treatment of interfacial behavior will lead to errors in the prediction of ultimate strength. Contact

modeling is typically avoided in day-to-day structural engineering analysis due to the computational expense associated with such considerations. However, since the geometry of the structure under investigation involves a flexible shell structure bearing against a rigid curved surface, it is difficult to exercise engineering judgment regarding the potential effects of contact in this case. Therefore, an analysis is performed with a true contact interaction (separation and sliding allowed) at the interface between the HSS chord and the saddle bearings. For this analysis, the saddle bearings are modeled as analytical rigid bodies. That is, they are considered to be infinitely stiff. This approximation is acceptable since any deformation of the saddles is negligible and will have almost no affect on the capacity of the system.

The contact analysis results indicate that while some minor localized sliding may occur between the HSS and the saddles, uplift does not occur as a result of the compressive nature of the loading. More importantly, the ultimate load determined by contact analysis is within 1% of the load when using the simplified boundary condition (but at significant increased cost in terms of analysis time). Thus, the simplified (fully pinned) boundary condition is deemed acceptable for the HSS/saddle interface.

13. Mesh density

In development of the final modeling techniques (i.e., S4R element in a mesh pinned at the saddle), a mesh convergence study is performed employing S4R element sizes of 50 mm, 25 mm, 12 mm, and 6 mm. It is determined that the accuracy of the solution is improved as the mesh size is refined, but the improvement between 12 mm and 6 mm is insignificant in comparison to the increased run time. Thus, the recommended element size for the S4R element is 12 mm, which is used throughout the model.

14. Material model

Since the global failure mechanism observed involves plastification of the chord wall into well-defined yield lines exhibiting large strains (i.e., greater than 1%), the material model that is used to describe how the structural components will deform is vital to obtaining accurate overall results. Unfortunately, the material behavior, as opposed to geometry, loading and boundary conditions, is where the greatest uncertainties lie.

The basic form of the material definition utilized is consistent with that of a von Mises metal plasticity model and an associated plastic flow rule. In general, metals resist a portion of a large externally applied load through the development of an elastic strain potential. The remaining portion of the external work is then dissipated through the action of internal plastic work. For the case of mild steel, the primary mechanism for this is plastic flow occurring along slip planes. This slipping coincides with atomic structural imperfections such as crystal dislocations and sites of non-metallic impurities in the metallic grains.

The foundation of the von Mises theory is the assumption that metallic materials resist all hydrostatic stress in an elastic fashion. Thus, only the deviatoric components of the stress state are associated with the initiation and propagation of plastic flow, which has been confirmed experimentally for most common metals (ABAQUS 2003). This assumption leads to the development of a *yield function* or *yield surface*, which defines the limit of purely elastic response as well as the direction of plastic flow

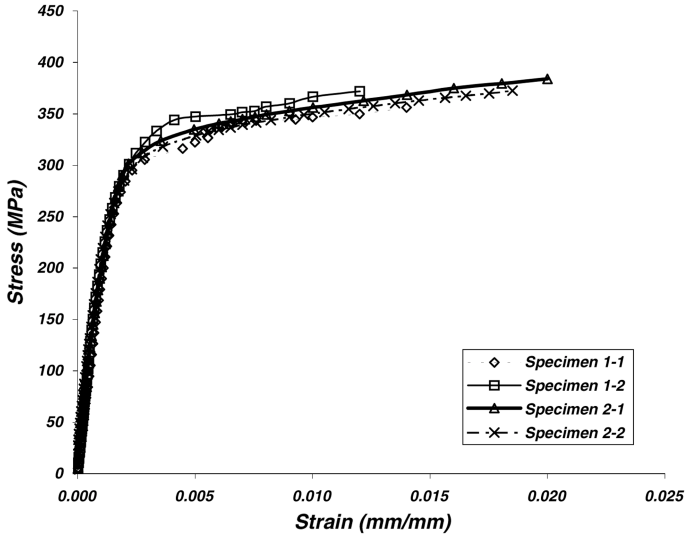

Fig. 7 Coupon test results from HSS steel

for 3D stress states. The assumed direction of plastic flow is the same as the direction of the outward normal to the yield surface, which is often referred to as *associated flow.* Associated flow models are useful for materials in which dislocation motion provides the fundamental mechanisms of plastic flow (ABAQUS 2003). To define the material for the finite element analysis model, only the uniaxial behavior need be employed; ABAQUS will use this data to generate the required von Mises yield surface in 3D stress space.

For the uniaxial material definition, coupon test results from the actual test specimens are used. Two (2) coupons are cut and tested from each of the HSS chords in the test specimens, yielding a total of four (4) tests, which are all shown in Fig. 7 (Boyle and Earls 2004). Due to difficulties in machining coupons in the transverse direction of the HSS (see discussion above), only coupons from the longitudinal direction are taken. To utilize the coupon test data for the material model definition, it is assumed that the steel is isotropic, linear-elastic with isotropic plastic hardening and rate and temperature independence. That is, the response is assumed to be linear up to a discrete yield point, after which plastic (permanent) deformation occurs as described by a work hardening curve with no influence from temperature or strain rate. The elastic modulus is determined to be 145 GPa (21,000 ksi) by taking the average tangent value in the elastic range, and the yield point is established utilizing the standard 0.2% offset method to be 310 MPa (45 ksi). The work hardening curve is defined using a piecewise linear function developed from the actual measured coupon test data. It should be noted that for large deformation finite element analysis analysis, “engineering” stress and strain must be converted to “true” stress and logarithmic strain using the following relationships:

$$\varepsilon_{true} = \ln (1 + \varepsilon_{eng}) \tag{1}$$

$$\sigma_{true} = \sigma_{eng} (1 + \varepsilon_{eng}) \tag{2}$$

The results from Eqs. (1) and (2) are then included in the ABAQUS input deck in order that a failure surface may be constructed in three dimensional stress space.

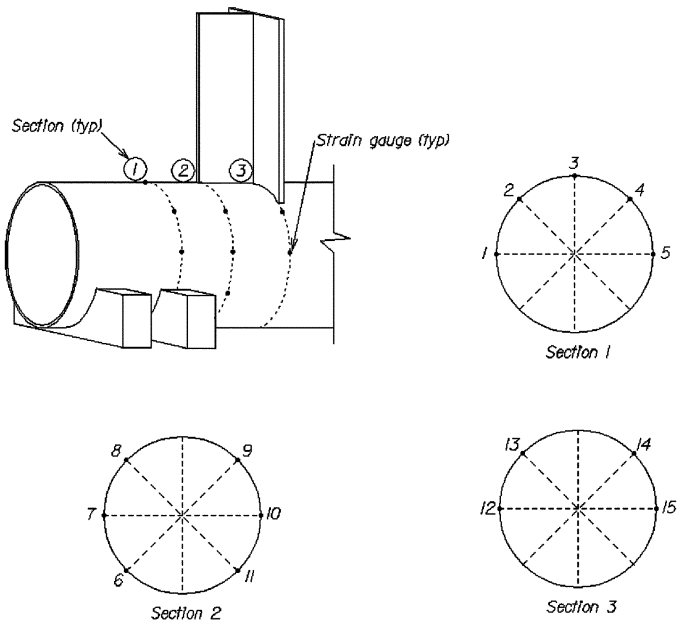

Fig. 8 Rosette strain gauge locations

15. Verification of finite element analysis techniques

To verify that the modeling techniques are producing accurate results, a full simulation of the experimental testing carried out at the University of Pittsburgh is performed and the analytical results are compared to the experimental measurements. Specifically, the deflections recorded by the displacement transducers (DCDTs) and the strains measured by the rosette gauges installed on the surface of the HSS chord wall are compared to the finite element analysis results.

The DCDT measurements that are used for the verification are designated as DCDT 1 and DCDT 2 from the experimental test data (see Fig. 2). DCDT 1 measured the total displacement at the point of load application (including both global and local deformation effects within the specimen) and DCDT 2 measured the local deformation (ovalization) of the HSS cross section at the open end.

Strains measured with rosette gauges on the surface of the HSS chord wall are also used for verification of the finite element analysis modeling techniques. These gauges were positioned uniformly along the circumference of the HSS chord in three (3) sections between the ST and saddle bearings. The gauge locations and their respective numbers are shown in Fig. 8.

16. Overall agreement

First, the overall specimen behavior and response is discussed in the context of the observed evolution in the failure modes. As noted in the observations of the experimental results at failure, dimples form in the HSS wall around the ST flange tips and the open end of the HSS deforms into an oval shape (Boyle and Earls 2004). A deformed shape consistent with this description is also predicted by the finite element analysis based simulation (see Figs. 9(a)-(d)). In addition, a number of rosette

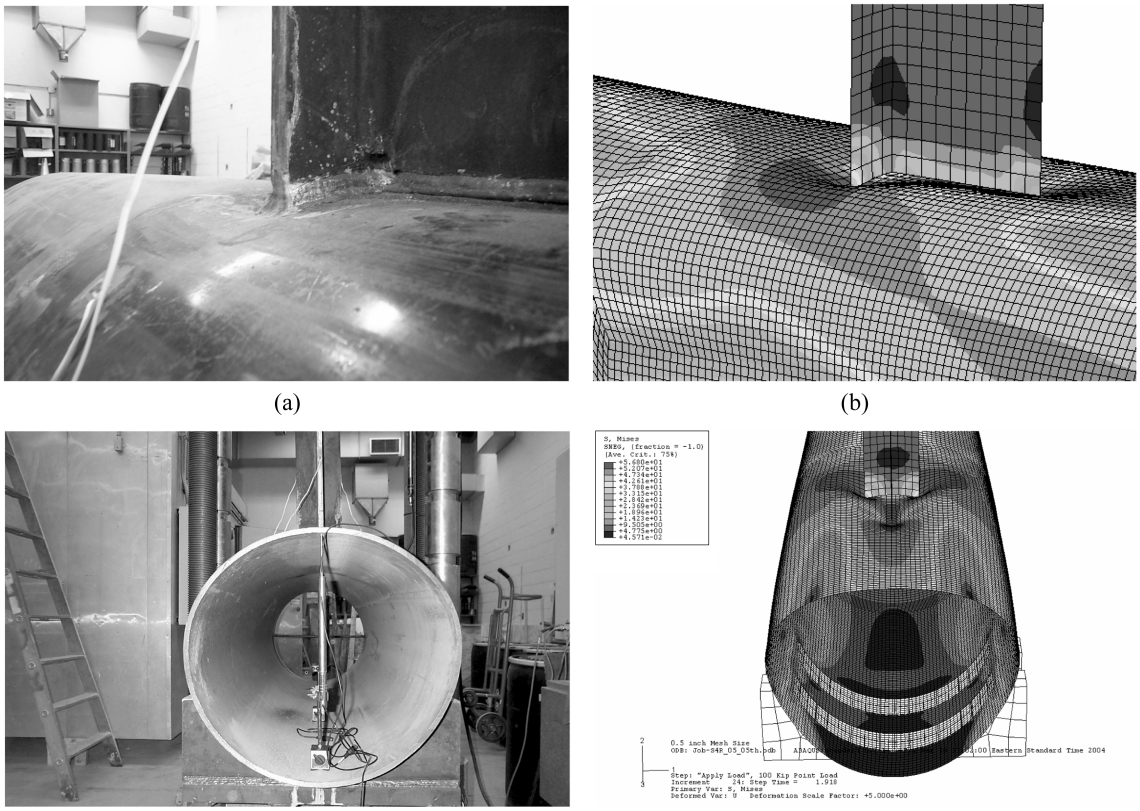

Figs. 9 Deformed shape comparison: (a)(b) dimpling under ST and (c)(d) ovalization at end

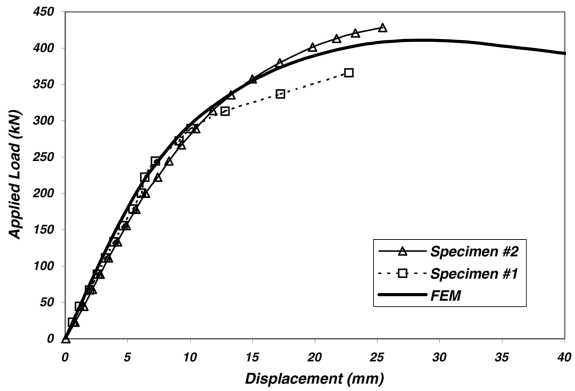

Fig. 10 Load-deflection response comparison at applied load (DCDT 1)

gauges indicate yielding in the HSS chord wall during testing: they are gauges 1, 3, 5, 8, 9, 13, and 14. In general, these locations of yielding are consistent with the yield line patterns as discernable in the exhibited von Mises stress contours presented in Fig. 5. In general, these initial observations indicate that the same basic mechanisms of failure are being captured.

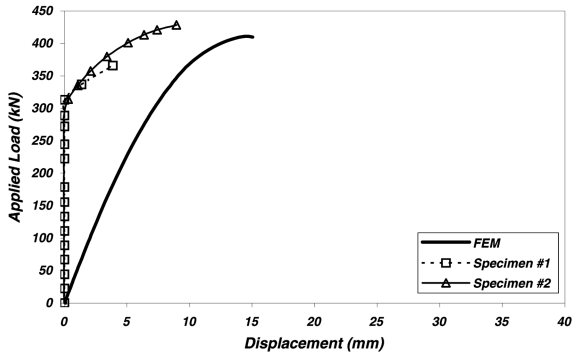

Fig. 11 Load-deflection response comparison at HSS end (DCDT 2)

17. Agreement in displacements

Next, the displacements from the finite element analysis and experimental results are compared. By studying the global deflection at the point of load application in Fig. 10, it can be seen that the agreement between the experimental results and finite element modeling results appears to be favorable at this location. Recall that this is the DCDT 1 measurement discussed previously. The elastic stiffness (initial slope of the load-deflection curves) is consistent and the peak loads from the finite element analysis and experimental results of Specimen #2 are within 4%; 411 kN (92.4 k) vs. 428 kN (96.3 k). It is also noted that these ultimate loads occur at nearly the same deflection; this may be important if one desired to use a deflection criterion for defining the nominal capacity in a design context. One minor difference to note is that the finite element analysis predicts a slightly softer response in the inelastic range; i.e., the load above 267 kN (60 k). This results in a slightly lower ultimate load predicted by finite element analysis as compared to the experiment, but still within a small percentage of the total load.

Additionally, the displacements at the open end of the HSS are compared (see Fig. 11). Since this location is 840 mm (33”) away from the ST strut, the deflection here indicates to what extent the applied load is dispersed longitudinally in the chord wall. Interestingly, both experiments showed no movement until a load of 311 kN (70 k), at which point the open end closed quickly. In contrast, this response is not predicted by the finite element analysis. The finite element analysis results indicate a gradual (smooth) increase in deflection from the beginning of load application up to a maximum deflection of 15 mm (0.6”).

18. Agreement in strains

Since strains are the actual measured data from the gauges (and thus do not require any additional assumptions regarding material mechanical behavior), comparisons based on these measures represent the most direct approach for determining agreement between the models and the physical tests. However, strains are often difficult to correlate between experiment and analysis since strain is defined at an idealized material point in space. This type of measurement is a simple matter for a computer model based on the finite element method, but in a real physical test, the strain rosettes tend to be quite large in size and thus the strain measurements are effectively being averaged over significant gauge lengths in the lab testing. Also, strain measurements tend to be very sensitive to the residual stresses and variations in the thickness in the base material.

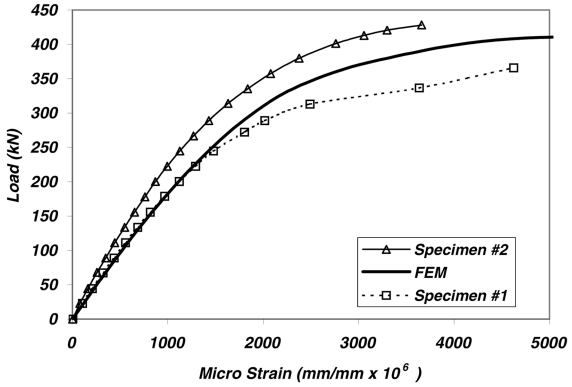

Fig. 12 Principal strain comparison at gauge location 3

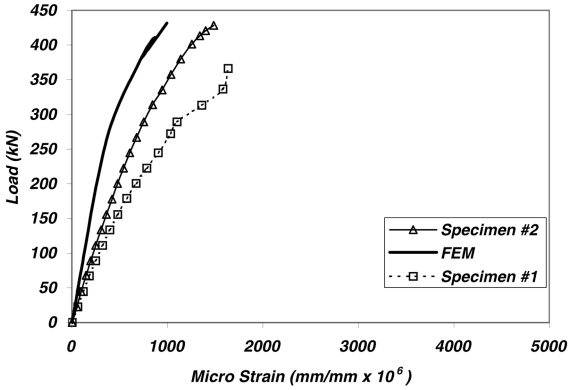

Fig. 13 Principal strain comparison at gauge location 5

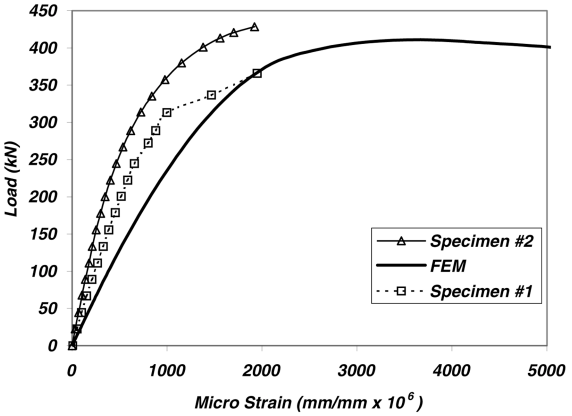

Fig. 14 Principal strain comparison at gauge location 9

The locations considered in this portion of the comparison in results are all the locations where yielding of the HSS wall occurs; these locations tend to exhibit large magnitudes of strain, which are more useful for comparison purposes. Since rosettes 1, 8, and 13 are mirror locations about the

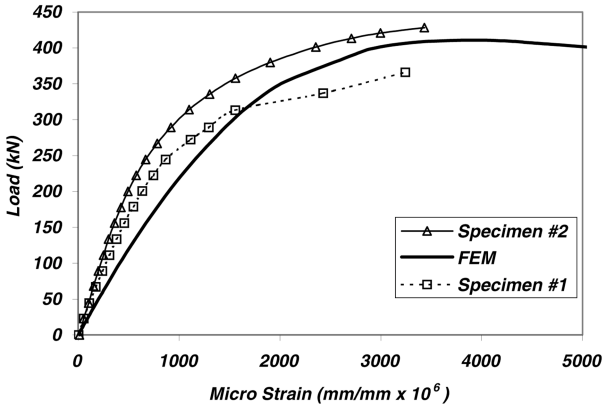

Fig. 15 Principal strain comparison at gauge location 14

CL of the HSS to rosettes 5, 9, and 14 respectively, symmetry is exploited and only one-half of the instrument readings are considered. It should be noted that the mirror locations all showed similar behavior to their associated rosette on the opposite side. This indicates that the experimental loading and response was symmetric; with no significant out-of-plane bending or twisting of the specimen.

The comparisons of the principal strains at the four (4) yielded locations are shown graphically in Figs. 12-15. By studying the figures, it can be seen that the finite element analysis and experimental strains agree very well at rosettes 3 and 14. The initial slope of the curves, the load at which the curves become nonlinear, and the strain magnitude at the peak load are all relatively consistent. Of all the rosettes, these two locations exhibited the largest magnitude of total strain: in the range of 3500-4500 microstrains (the uniaxial yield strain is approximately 2200 microstrains). Large strains are expected here since rosette 3 is located at the apex of the HSS adjacent to the ST web where a yield line is well defined. Large strains are also expected at rosette 14 since this is in close proximity to the ST flange tip where significant dimpling was observed in the specimens. For rosettes 5 and 9, the comparisons are slightly less favorable, but are still very reasonable. The less favorable agreement observed between modeling results and physical testing results is likely due to the fact that the magnitudes of the strains are smaller than those observed at 3 and 14, and so any discrepancies are more pronounced in terms of gross percentages of measured response.

19. Discussion of results

Overall, the agreement between the finite element analysis results and the experimental tests is favorable. The finite element analysis based simulation supports the general observations made during the testing, and the displacement and strain measurements taken from the specimens are mostly consistent with the analytical results. Thus, it is concluded that the finite element analysis techniques employed herein are valid for analysis of the structure under investigation. However, from this research, a number of issues with regard to finite element analysis of tubular steel structures have arisen which are discussed in more detail below.

20. Sources of discrepancy

The potential sources of discrepancies between the finite element analysis and experimental results are: physical variations in HSS wall thickness, diameter, mass, and residual stresses as discussed previously. However, since actual measurements of these properties were not taken from of the specimens, it is difficult to ascertain their exact influence. These items will be discussed in a general sense by assuming that the magnitudes are consistent with other manufactured HSS members and in light of the tolerance values specified by ASTM A53. It is pointed out right away that, in general, the strains computed using the finite element method are less accurate than the nodal displacements in the context of a given mesh. This is due to the fact that the displacements are nodal quantities that are solved for directly in each equilibrium iteration. In contrast, the stresses are obtained from engineering theories applied at the mid-surface Gauss points and subsequently extrapolated out to the nodal locations. As a result of this extrapolation, the strains predicted with the finite element model are somewhat less accurate than the displacements predicted with the same model.

As mentioned, the strain measurements on the chord wall surface are very sensitive to residual stresses and local variations in wall thickness. Residual stresses will not only result in a change in the localized yielding response, but could also cause a global redistribution of the applied loads in the form of shift in the trajectories of the yield line patterns. Note that in the present discussion, the strains are compared in terms of principal strain, which means that both longitudinal and transverse residual stresses will influence the onset of yielding. However, from Figs. 12-15, it is observed that there are not significant differences in the yielding behavior. That is, the initiation of nonlinear behavior is relatively consistent between finite element analysis and the experiments. The differences that exist are more in terms of overall magnitude at a given load, which is more attributable to a yield line shift. If the actual yield lines deviate from the theoretical patterns, this would have a more significant impact on the strain magnitude at discrete gauge locations.

Variations in wall thickness will also result in a change in the extreme fiber strain as compared to the idealized finite element analysis model, which uses the nominal thickness. By considering the linear strain distribution from fundamental flexural theory, the strain for a given elemental curvature is directly proportional to the distance from neutral axis. Thus, a 10% variation in wall thickness (as per ASTM) would result in a 10% variation in extreme fiber strain. This may partially explain the differences in strain magnitude between finite element analysis and the experiments, but some differences are much larger than this.

The most significant difference found in the comparison of finite element analysis vs. experimental results is in the displacement response at the open end of the HSS chord. As discussed previously, in the experiments the open end showed no movement until a load of 311 kN (70 k). In contrast, a gradual distortion of the open end was observed in the finite element models. This difference in response is likely not the result of a modeling issue since the other displacements and strains compare so well. Also, it cannot be attributed to residual stresses and/or dimensional tolerances from the HSS chord manufacturing processes, since neither would have such a dramatic influence on how the applied load is dispersed longitudinally in the chord wall.

Since the experimental researchers noted that a moment was present in the ST strut and that shims for the load frame became loose and fell out during testing of both specimens (Boyle and Earls 2004), it is likely that there existed some unknown flexibility and/or restraint in the testing setup which would be a deviation from the ideal boundary conditions used in the analytical modeling.

Another possibility is that the HSS steel is textured, resulting in different material stiffnesses (moduli) for the longitudinal and transverse directions. Recall that coupon tests were conducted in the longitudinal direction only, and thus the circumferential behavior is unknown. To explore this possibility, a finite element analysis is conducted using an orthotropic material definition with E_{long} = 145 GPa (21,000 ksi) and E_{circum} = 200 GPa (29,000 ksi), which is chosen arbitrarily. From this analysis, it is determined that a textured steel would reduce the theoretical end displacement, which agrees more favorably with the experimental results. However, while it is that texturing may be influencing the physical behavior, it is difficult to fully ascertain to what extent this may be the case.

21. Failure mechanism

The mechanism of failure for this structure is an example of a yield line collapse mechanism in which well-defined plastic hinge lines develop in the HSS chord walls, causing instability at a critical load. This is defined as the point at which the tangent stiffness (slope of the load-deflection curve) equals zero. The yield lines exhibit a geometry that is somewhat complex due to the asymmetry of the ST connection and the proximity to the open end of the HSS. However, based on the good agreement between finite element analysis and the experiments in terms of global load-deflection response, the salient features of the governing failure mechanism appear to be captured sufficiently well in the analytical modeling.

The present discussion now shifts focus to two specific points: 1) the stiffness after yielding, and 2) the magnitude of the ultimate load; both of these are related to residual stresses in the HSS chord. The residual stresses present can affect both the mechanism geometry (i.e., shifting of the yield lines) and the local plastic hinge capacity. Based on Fig. 4, the longitudinal residual stresses in an HSS member may approach the yield stress in the vicinity of the welded seam. Although this is significant in terms of magnitude, the yield line mechanism for this structure consists mostly of lines oriented longitudinally. Such yield line orientations are not significantly impacted by longitudinal residual stresses in terms of unit strength. However, the longitudinal weld seam might cause a shift in the yield line location. Since any deviation from the ideal (theoretical) mechanism will have a net strengthening effect and result in a higher capacity, this would explain the slightly larger experimental ultimate load.

In contrast, the transverse residual stresses directly influence the net unit capacity of the longitudinal yield lines. From Fig. 4, the circumferential residual stress distribution is nearly linear, and resembles the stress distribution from simple flexural theory. Thus, the residual stress can be thought of as a residual moment of approximate magnitude $M_{residual}=\sigma S$, where σ =0.35 σ_y and S is the section modulus per unit length of chord wall. For this structure, the residual moment is calculated:

$$M_{residual} = (0.35 \cdot 310\text{MPa}) \cdot (1\text{mm} \cdot (12.7\text{mm})^2/6) = 2.92\text{kN} \cdot \text{m/m}(0.656\text{k} \cdot \text{in/in}) \quad (3)$$

From simple plastic section analysis, the plastic moment resistance of the chord wall per unit length is $F_y t^2/4$ which yields:

$$M_p = (310\text{MPa}) \cdot (12.7\text{mm})^2/4 = 12.5\text{kN} \cdot \text{m/m}(2.81\text{k} \cdot \text{in/in}) \quad (4)$$

Thus, there exists a residual moment that is 2.92/12.5=23% of the plastic moment resistance, which could have a stiffening or softening effect depending on the direction of the applied flexure. It must

be noted that this residual moment will affect the onset of yielding and the inelastic response for the collapse mechanism, but it will not affect the ultimate load since plastic moment resistance is independent of residual stress. Thus, the circumferential residual stress might explain the difference in tangent stiffness observed in the inelastic range.

22. HSS material modeling

As discussed previously, modeling of the HSS material is where the greatest uncertainties lie. It is likely that the steel in the test specimens contained residual stresses and was somewhat textured as a result of the manufacturing processes; but these internal properties are difficult to quantify for the purposes of analytical modeling. Thus, neither was utilized in the material definition for the finite element analysis model. However, it is believed that both may have contributed to observed differences in predicted versus observed responses throughout the verification study.

To transform a flat plate into a circular tube, significant circumferential strains will result. Based on the assumption of plane sections remaining plane from fundamental flexural theory, a plate of thickness "t" bent into a curve of radius "R" will have extreme fiber strains given by the relationship $\varepsilon = t / 2R$. For the test specimen chords, this results in maximum strains of ε = (12.7 mm) / 2(330 mm) = 0.0192 mm/mm, which is over ten times the yield strain ε_y. Thus, it is likely that some level of texturing has occurred and the properties of the steel are different in the longitudinal and transverse directions. However, coupon tests were conducted in the longitudinal direction only, and thus the significance of the texturing could not be quantified precisely, but it was clear that the longitudinal elastic modulus was somewhat less that the 200 GPa (29,000 ksi) typically ascribed to steel.

In defining the material model, the von Mises metal plasticity model is utilized, which assumes that the stress-strain response is linear up to a discrete yield point. However, in studying the coupon test data closely it is observed that the material response is nonlinear throughout the elastic range, which is consistent with the findings of Toma and Chen (1979), but even more pronounced. To minimize the error from this linear approximation, an average elastic modulus of 145 GPa (21,000 ksi) was specified for the model as opposed to the initial tangent value from the coupon test results. This results in the most favorable agreement in the load-deflection response.

23. Conclusions

This paper reports on finite element analysis techniques that may be applied to the study of circular hollow structural sections and related bearing connection geometries. The modeling is carried out in conjunction with a program of experimental testing that has been conducted on a tubular truss bearing region. The significant findings and/or recommendations are:

1) The finite element modeling techniques produce results that agree well with displacement and strain measurements taken from two (2) experimental tests and thus are considered to be verified for future parametric studies on tubular truss bearings.
2) A linearly interpolated, quadrilateral shell element that employs a general-purpose formulation and reduced integration is the recommended finite element type for modeling of the structure under investigation. Since the demands on the shell are mostly flexural, this problem could be solved

adequately using a simplified thin shell element. However, a general-purpose element that considers finite membrane strains displays a slightly better agreement with experimental results and is deemed more favorable for future parametric studies that aim to use the geometry reported on herein as a point of departure.

3) A simplified boundary condition at the saddle bearings, as opposed to a true contact interaction, is sufficiently accurate for modeling of this structural type.
4) Tubular (HSS) members have somewhat loose dimensional tolerances governing their manuacturing and also contain significant residual stresses as a result of the manufacturing processes; both require that analytical modeling of the steel material properties be done with great care.
5) The global failure mechanism observed in both the experimental tests and the finite element analysis involves a flexural collapse of the HSS chord through plastification of the chord wall into a well-defined yield line mechanism. Thus, the yield line method is the recommended approach for predicting capacity.

References

ABAQUS, (2003), *ABAQUS Theory Manual*, Hibbitt, Karlsson & Sorensen, Inc., Pawtucket, Rhode Island, USA.

AISC (2000), Load and Resistance Factor Design Specification for Steel Hollow Structural Sections, *American Institute of Steel Construction*, Chicago, Illinois, November 10.

AISC (2001), Manual of Steel Construction - Load and Resistance Factor Design 3rd Edition, *American Institute of Steel Construction*, Chicago, Illinois, November.

AISC (1997a), Hollow Structural Sections Connections Manual, *American Institute of Steel Construction*, Chicago, Illinois.

AISC (1997b), Specification for the Design of Steel Hollow Structural Sections, *American Institute of Steel Construction*, Chicago, Illinois, April 15.

Bathe, K.-J. (1996), *Finite Element Procedures*, Prentice-Hall, Inc., Upper Saddle River, New Jersey.

Boyle, R. and Earls, C.J., (2004), "Full-scale testing of tri-chord sign structure connections", Report No. CE/ST 28, Department of Civil and Environmental Engineering, University of Pittsburgh, Pittsburgh, Pennsylvania.

Chen, W.F. and Ross, D.A. (1977), "Tests of fabricated tubular columns", *J. Struct. Div.*, ASCE, **103**(ST3).

Dieter, G. E. (1986), *Mechanical Metallurgy* 3rd Ed., McGraw Hill, ISBN 0-07-016893-8.

Galambos, T. (1998), *Guide to Stability Design Criteria for Metal Structures*, 5th Ed., Wiley, ISBN 0471127426.

Greco, N. and Earls, C.J. (2003), "Structural ductility in hybrid high performance steel beams," *J. Struct. Eng.*, **129**(12), American Society of Civil Engineers, Reston, Virginia, 1584-1595.

Kurobane, K., Makino, Y. and Mitsui, Y. (1976), "Ultimate strength formulae for simple tubular joints", IIW Doc. XV-385-76. Dept. of Architecture, Kumamoto Univ.

Kurobane, K., Makino, Y. and Mitsui, Y. (1980), "Re-analysis of ultimate strength data for truss connections in circular hollow sections", IIW Doc. XV-461-80. Dept. of Architecture, Kumamoto Univ.

Kurobane, K. (1981), "New developments and practices in tubular joint design", IIW Doc. XV-488-81. Dept. of Architecture, Kumamoto Univ.

Li, Y. and Earls, C.J. (2002), "Design recommendations for the proportioning and detailing of long-span tri-chord sign structures, Phase I", Report No. CE/ST 24, Department of Civil and Environmental Engineering, University of Pittsburgh, Pittsburgh, Pennsylvania.

Packer, J.A. and Henderson, J.E. (1997), *Hollow Structural Section Connections and Trusses*, second edition, *Design Guide*, Canadian Institute of Steel Construction, Willowdale, Ontario, Canada, June.

Prion, H.G.L. and Birkemoe, P.C. (1988), "Experimental behaviour of unstiffened fabricated tubular steel beam-columns", Publ. No. 88-3, Department of Divil Engineering, University of Toronto, Toronto, Ontario, Canada.

PENNDOT (2003a), "Overhead sign structures – 2-Post & 4-Post tri-chord truss spans from 18 288 to 73 152

(60' to 240') notes and design criteria", Standard Drawings for Bridge Design - BD 644-M, Commonwealth of Pennsylvania Department of Transportation, Harrisburg, Pennsylvania.

PENNDOT (2003b), "Overhead sign structures − 2-Post & 4-Post tri-chord truss spans from 18 288 to 73 152 (60' to 240') notes and design criteria", Standard Drawings for Bridge Construction - BC 744-M, Commonwealth of Pennsylvania Department of Transportation, Harrisburg, Pennsylvania.

Popov, E.P., Zayas, V.A., Mahin, S.A. (1979), "Cyclic inelastic buckling of thin tubular columns", *J. Struct. Div.*, **105**(ST11).

Thomas, S. and Earls, C.J., (2003), "Cross sectional compactness and bracing requirements for HPS483W girders", *J. Struct. Eng.*, **129**(12), American Society of Civil Engineers, Reston, Virginia, 1569-1583.

Toma, S. and Chen, W.F. (1979), "Analysis of fabricated tubular columns", *J. Struct. Div.*, ASCE, **105**(ST11).

Wardenier, J. (1982), *Hollow Section Joints*, Delft University Press, Delft, ISBN 90.6275.084.2.

Wardenier, J., Kurobane, Y., Packer, J.A., Dutta, D. and Yeomans, N. (1991), *Design Guide for Circular Hollow Section (CHS) Joints Under Predominantly Static Loading*. CIDECT (ed.) and Verlag TUV Rheinland GmbH, Koln, Federal Republic of Germany.

CC